Photoluminescence investigation of the indirect band gap and shallow impurities in icosahedral $B_{12}As_2$

P. B. Klein,[1] Ugochukwu Nwagwu,[2] J. H. Edgar,[2] and J. A. Freitas, Jr.[1]
[1]*Naval Research Laboratory, Washington DC 20375, USA*
[2]*Department of Chemical Engineering, Kansas State University, Manhattan, Kansas 66506, USA*

The indirect band gap of icosahedral $B_{12}As_2$ (IBA) has been determined by variable temperature photoluminescence measurements (8 K-294 K) on solution-grown bulk samples. In addition, evidence of three shallow acceptor levels and one shallow donor level is reported. The low-temperature spectra were characterized by broad and intense deep defect emission, donor-acceptor pair (DAP) bands, and exciton recombination. The appearance of DAP emission verifies the incorporation of a donor in IBA, which has not been reported previously. The temperature dependence of the free exciton (FE) intensity reflected a FE binding energy of 45 meV. The variation of the FE peak position with temperature was fitted with both Varshni and Pässler models to determine an expression for the temperature dependence of the indirect band gap. The resulting low and room temperature band gaps are $E_g(0) = 3.470$ eV and $E_g(294\,K) = 3.373$ eV, respectively. The latter is not consistent with previous reports of the room temperature band gap, 3.20 eV and 3.47 eV, derived from band structure calculations and optical absorption, respectively. The origin of these discrepancies is discussed. The DAP spectra reveal three relatively shallow acceptors with binding energies of $\approx$175, 255, and 291 meV, and a shallow donor with binding energy $\approx$25 meV. Although the identity of the individual acceptors is not known, they appear to be associated with the light-hole band. The small donor binding energy is suggestive of an interstitial donor impurity, which is suspected to be Ni. © *2012 American Institute of Physics.*
[http://dx.doi.org/10.1063/1.4729920]

I. INTRODUCTION

Icosahedral boron arsenide, $B_{12}As_2$ (IBA), is a wide bandgap semiconductor that exhibits unusual properties as the result of the bonding within the 12-atom boron icosahedron that is an integral part of its crystal structure.[1,2] One of its most interesting properties is the ability to "self-heal" under intense ionizing radiation that would render other materials amorphous.[2,3] Emin has argued[2] that this radiation hardness results from the unique three-center bonds between icosahedral boron atoms. The bond charge is retained on the icosahedron when a boron atom is displaced due to the radiation; thus resulting in a Coulomb attraction between the vacancy and interstitial that enhances defect recombination. IBA is also a hard material with a high melting temperature ($>$2000 °C). This unique combination of physical characteristics makes IBA a natural choice for applications that must withstand high temperatures or intense radiation, such as thermoelectrics, neutron detectors, and alpha- and beta-voltaics.[2]

While there has been sparse but continuing interest in the properties of IBA over the years, the material remains poorly characterized and will require significant progress in materials growth to realize its potential. Small bulk crystals prepared from a liquid Pd-B melt were grown in early measurements of the thermal conductivity of IBA.[4] Within the last several years, there has been renewed activity, mostly focused on growing epitaxial layers of IBA on Si (Ref. 5) and on 4H-, 6H- and 15R-SiC.[6–8] Whiteley *et al.*[9] have recently investigated the growth of bulk crystals from a Ni-B solution. In all of these studies, the focus of the material

characterization has been on structural properties, with x-ray diffraction,[7] transmission electron microscopy,[7,8,10] and Raman scattering[11,12] as the primary experimental probes.

Recently Gong *et al.*[13] reported on the fabrication and performance of an IBA/n-type 4H-SiC p-n junction device, where the IBA was p-type with a carrier concentration of roughly 10^{17} cm^{-3}. In fact, as-grown boron-rich semiconductors are generally p-type. This occurs because inter-icosahedral bonding is maintained when an As atom is replaced by a vacancy or either a B, group IV, or group VI atom, and the resulting hole on the As site leads to p-type conductivity.[2] For example, Xu *et al.*[14] demonstrated that the conductivity of high-resistivity p-type IBA epilayers grown on semi-insulating 6H-SiC could be effectively modulated by Si doping, resulting in p-type conduction with a $\times\,10^5$ reduction in the resistivity. Hall effect measurements on similar as-grown epilayers ($\approx$3 μm thick) also exhibited p-type conductivity with hole concentrations[15] in the range ($\approx 10^{13}$–10^{16}) cm^{-3}. Thus far, n-type conductivity has not been reported in IBA.

Other studies of IBA have focused on thermal properties (Seebeck coefficient, thermal conductivity[16]), calculations of the vibrational properties,[17,18] and band structure calculations,[19–22] which indicate that the band gap of IBA is indirect, with a conduction band minimum at the A-point of the Brillouin zone. Optical studies have been limited to Raman scattering;[23] early work by Slack *et al.*[24] on refractive index and optical absorption, where the indirect band gap was reported to be 3.47 eV at room temperature; infrared (lattice) absorption appearing in Ref. 17; and recent room

1. REPORT DATE **05 JUL 2012**	2. REPORT TYPE	3. DATES COVERED **00-00-2012 to 00-00-2012**
4. TITLE AND SUBTITLE **Photoluminescence investigation of the indirect band gap and shallow impurities in icosahedral B12As2**		5a. CONTRACT NUMBER
		5b. GRANT NUMBER
		5c. PROGRAM ELEMENT NUMBER
6. AUTHOR(S)		5d. PROJECT NUMBER
		5e. TASK NUMBER
		5f. WORK UNIT NUMBER
7. PERFORMING ORGANIZATION NAME(S) AND ADDRESS(ES) **Naval Research Laboratory,4555 Overlook Ave SW,Washington,DC,20375**		8. PERFORMING ORGANIZATION REPORT NUMBER
9. SPONSORING/MONITORING AGENCY NAME(S) AND ADDRESS(ES)		10. SPONSOR/MONITOR'S ACRONYM(S)
		11. SPONSOR/MONITOR'S REPORT NUMBER(S)
12. DISTRIBUTION/AVAILABILITY STATEMENT **Approved for public release; distribution unlimited**		
13. SUPPLEMENTARY NOTES		
14. ABSTRACT		
15. SUBJECT TERMS		

16. SECURITY CLASSIFICATION OF:			17. LIMITATION OF ABSTRACT	18. NUMBER OF PAGES	19a. NAME OF RESPONSIBLE PERSON
a. REPORT **unclassified**	b. ABSTRACT **unclassified**	c. THIS PAGE **unclassified**	**Same as Report (SAR)**	**13**	

temperature spectroscopic ellipsometry measurements by Bakalova *et al.*,[21] which provided information on the dielectric function and interband critical points. The combination of this ellipsometry data with first principles band structure calculations[21] enabled critical point assignments and the determination of the required self-energy correction (≈ 0.6 eV) for the calculated direct band gaps. No experimental data were available near the indirect gap due to competing impurity absorption. Consequently, the fundamental band edge was determined by adding the self-energy correction obtained for direct transitions to the calculated indirect gap (2.56 eV), leading to a band gap of ≈ 3.2 eV. This band structure calculation also provided the first determination of the electron and hole effective masses for IBA.[21]

Thus, there are two very different values in the literature for the indirect band gap of IBA: 3.20 eV (Ref. 21) and 3.47 eV.[24] In this work, we address this issue by carrying out photoluminescence (PL) measurements over a broad temperature range. It is somewhat surprising that PL spectroscopy has not been reported previously for IBA, since the material has been of interest for at least 40 years. Optical characterization such as PL can provide information on the semiconductor band gap and on the defects and impurities that define or limit its transport properties. Since the existing values for the indirect band gap were measured at room temperature, while PL spectral features are more easily identified at low temperatures, the present measurements are carried out over the full temperature range between 8 K and 294 K.

II. EXPERIMENTAL

The IBA crystals were grown by the procedure described in detail by Whiteley *et al.*[9] In a sealed quartz tube, boron and nickel were placed in a boron nitride boat at one end, and arsenic was placed at the other end. The base pressure in the quartz tube before sealing is typically 5×10^{-6} torr. To begin the crystal growth, the zone containing boron and nickel alloy was heated to 1150 °C within 1 h and held at this temperature for 120 hours. The opposite end of the quartz tube that originally contained the arsenic was slowly heated up to 600 °C, where it was held for 120 hours. Crystal growth was initiated by slowly cooling to 1000 °C at a rate of 2 °C/h. The furnace was then turned off, and the quartz tube was allowed to naturally cool to room temperature.

Material growth was carried out with both low and high purity source materials. Crystals from the low-purity growth generally contained significant concentrations of metallic and nonmetallic impurities. To grow the high purity IBA crystals, care was taken to use all high purity source materials: The boron was 99.9999% pure, isotopically enriched boron-11, the arsenic was 99.99999% pure (metals basis), and the high purity nickel used had C, O, and Si concentrations of less than 50, 70, and 1 ppm respectively.

After the growth process, the crystallized $B_{12}As_2$ was then removed from the matrix by etching away the nickel in aqua regia at room temperature. The low purity IBA crystals were generally dark gray or black, and opaque. Many of the high purity IBA crystals were also dark gray, or black, and opaque, but some of the thinnest crystals were clear and transparent.

TABLE I. Impurity concentrations measured in IBA crystals by glow discharge mass spectrometry.

Impurity	Growth from low purity sources: Sample C		Growth from high purity sources: Samples A and B	
	Concentration		Concentration	
	ppm	cm^{-3}	ppm	cm^{-3}
Si	400	3.0×10^{19}	11	8.3×10^{17}
Ni	260	9.4×10^{18}	2200	8.0×10^{19}
S	89	5.9×10^{18}	<0.5	$<3.3 \times 10^{16}$
Er	25	3.2×10^{17}	<0.15	$<1.3 \times 10^{15}$
Se	12	3.2×10^{17}	<1	$<2.7 \times 10^{16}$
P	6.5	4.5×10^{17}	1.4	9.6×10^{16}

Three samples were employed in this study: Samples A and B were grown using the high purity sources while sample C was grown using the lower-purity sources. The impurity levels for both low purity and high purity IBA crystals were measured by glow discharge mass spectrometry and are shown in Table I. While the concentrations of most impurities dropped dramatically when the high-purity sources were used, this was accompanied by about an order of magnitude increase in the incorporation of Ni.

Photoluminescence measurements were carried out with the samples placed inside a variable temperature optical cryostat. Excitation was provided by ≤ 20 mW of 325 nm light from a He-Cd laser. The emitted radiation was collected and focused into a 0.85-m double spectrometer employing 1800 gpm gratings and was detected by a cooled GaAs photomultiplier. The spectral bandpass was usually set at ≈ 2.2 meV.

III. RESULTS AND DISCUSSION

A. Overview—low temperature photoluminescence spectra

Low temperature PL spectra taken over a broad energy range are shown in Fig. 1 for the two high-purity samples A (dotted line) and B (dashed line) as well as for the low-purity sample C (solid line). The dominant spectral features are
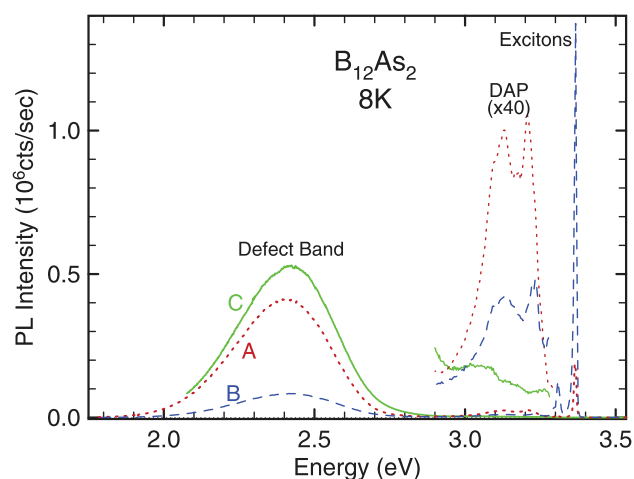

FIG. 1. Low temperature PL spectra of the two high purity samples A (dotted line) and B (dashed line) and the low purity sample C (solid line).

remarkably similar to those observed in other wide bandgap semiconductors, such as GaN, which is usually dominated by a broad and intense deep defect band, a donor-acceptor pair (DAP) region, and a near-gap region dominated by excitonic recombination. In the IBA spectra of Fig. 1, a broad, deep defect-related band is observed centered at 2.4 eV. In the following sections, we will discuss in detail the excitonic recombination from IBA, represented in Fig. 1 by the two sharp emissions at 3.309 and 3.366 eV and DAP recombination observed in the range 3.2–3.4 eV in the figure. Comparing the spectra of the two high-purity samples, sample A exhibits much stronger defect and DAP emission and much weaker exciton recombination than sample B, indicating that sample B is of higher quality. The low-purity sample C exhibits only a very intense defect band and no exciton-related emission, which is consistent with a very high concentration of defects and/or impurities.

The PL spectra from all three samples exhibited significant spatial inhomogeneity, as the spectra varied substantially when the exciting laser spot was moved over the samples. This inhomogeneity was also confirmed through PL imaging measurements and was evident from the overall spatial variation in the spectra. The data presented in the rest of this work were always obtained from the high-quality region of each sample, characterized by a maximum exciton emission intensity and a minimum defect band intensity.

Broad and intense defect/impurity bands emitting well below the band gap appear to be a common feature in the PL spectra of wide band gap semiconductors. The width and general lineshape of the ≈2.4 eV emission observed from IBA is reminiscent of the ≈2.25 eV "yellow band" in GaN, which is thought to be a carbon-related defect,[25,26] and the broad ≈2.4 eV emission in n-type 4H-SiC related to a deep boron-complex center.[27] Determining the nature of the defect responsible for these emissions requires a study of the effect of impurity and/or defect concentrations on the PL spectrum. While these measurements have not been carried out in IBA, from Table I, it is evident that sample C contains an order of magnitude less Ni and considerably higher concentrations of all other impurities as compared to samples A and B. While this suggests that the high concentration of Ni is not responsible for the quenching of the exciton emission in sample C, it is more likely that the strong exciton PL in samples A and B arises from the high-quality region of each sample, which contains a much lower Ni concentration. There is also a large variation in the defect- and exciton-related PL intensities of the two "high purity" samples A and B, which makes it difficult to make more meaningful correlations between the relative PL intensities and the level of impurities in these samples.

B. Bound exciton spectra

At very low temperatures, optical excitation produces photoexcited electron-hole pairs that rapidly form free excitons which are just as rapidly captured at (usually neutral) impurities, forming bound excitons (BEs). Until the temperature is raised, the BE state is the most stable configuration for the carriers. The bound exciton can annihilate by recom-

bining radiatively, as BE PL, or it can dissociate thermally, leaving a neutral impurity and either a free exciton or a free electron-hole pair. While these two dissociation mechanisms are most common, others involving either Auger recombination and/or a change in the charge state of the impurity are also possible.[28–30] As we do not have reliable information of the carrier type or compensation level of the samples investigated here, the bound excitons can be associated with neutral or possibly ionized donors or acceptors.

The dominant sharp line at 3.366 eV in Fig. 1 is identified as an exciton bound to a shallow impurity, or "shallow bound exciton" (SBE), based not only on its relatively narrow line width and its position in the spectrum but also from its temperature dependence, which is discussed in Sec. III C. The SBE line is shown in more detail as the solid line in Fig. 2(a). Because IBA is an indirect band gap semiconductor, it was not initially clear whether this intense emission band was a zero-phonon line (ZPL) or resulted from a phonon-assisted transition. However, a very weak emission suspected of being the ZPL for this band was observed at 3.419 eV, shown magnified by 500X in Fig. 2(a). To verify its origin, the slow-varying background was subtracted from the
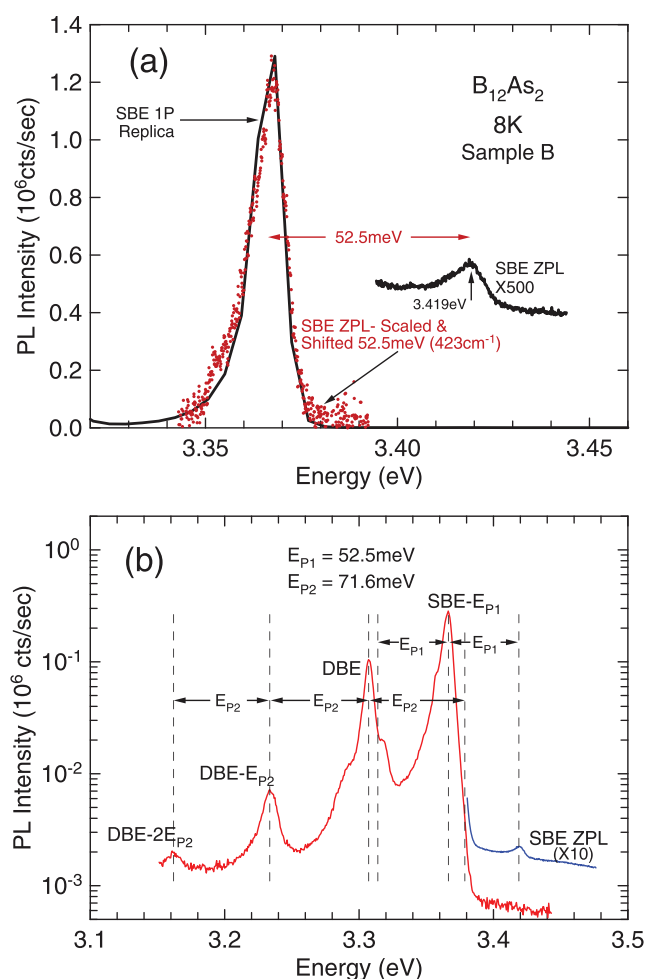

FIG. 2. (a) Low temperature PL spectrum of the 3.366 eV SBE (solid line) compared to the scaled and shifted weak emission at 3.419 eV (dots). (b) Log-intensity plot of the low temperature PL in the exciton region. The DBE exhibits two phonon replicas separated by $E_{P2} = 71.6$ meV, while a weak SBE ZPL and a strong 1-P replica at 3.366 eV are observed.

spectrum, the intensity was scaled to that of the BE line, and the band was shifted down in energy by $E_{P1} = 52.5$ meV to coincide with the BE. The resulting spectrum (dots) in Fig. 2(a) is almost identical to that of the BE line (solid line), verifying that this weak emission is the SBE ZPL and that the dominant emission is a one-phonon (1-P) replica involving a 52.5 meV (≈ 423 cm^{-1}) momentum-conserving (MC) phonon.

Hence, the main SBE PL transition appears to be phonon-assisted. Dipole selection rules require that the MC phonons be of odd symmetry. Fan[18] has recently calculated phonon dispersion relations for IBA. Of the 42 possible modes, 10 infrared active "u" modes were identified: $4A_{2u} + 6E_u$. One of the zone center E_u modes, calculated at 486 cm^{-1} and observed in infrared absorption at 483 cm^{-1},[31] was found by Fan to split into two modes along the Γ-A direction, appearing near 506 cm^{-1} and 406 cm^{-1} at the A-point. Although BE recombination does not always require phonon assistance, in this case, it appears that the lower of these two A-point phonons may well be involved.

In Fig. 2(b), the spectrum of the full exciton region is shown on a log-intensity scale, so that all significant features can be more clearly seen. After the intense SBE line at 3.366 eV, the next dominant feature is located at 3.309 eV, 57 meV lower in energy. This feature can be seen in Fig. 2(b) to have two further phonon replicas, both separated by about $E_{P2} = 71.6$ meV (≈ 578 cm^{-1}). If the 3.309 eV band is a one-phonon replica, then a ZPL would be expected at 71.6 meV higher energy, at 3.381 eV. This occurs near the high energy edge of the SBE emission, as indicated in Fig. 2(b). After careful study of this spectral region, no PL feature was detected at this energy, suggesting that the DBE line is a ZPL. As we will show in Sec. III D, this corresponds to a DBE about 116 meV below the exciton gap. If the transition were phonon assisted, this would be reduced by E_{P2} to ≈ 44 meV. These are large BE localization energies. Such deep bound excitons (DBEs) are often associated with transition metal impurities.[32–34] Thus, the high Ni content in these samples suggests the possibility that the DBE emission could result from excitons bound to a deep Ni-related center. The DBE line also exhibits weaker shoulders at lower and higher energy. While the higher energy feature is close to one phonon energy below the SBE line and could be a second phonon replica, the lower feature remains unidentified.

The SBE line at 3.366 eV participates with a 423 cm^{-1} phonon in the indirect transition, while the DBE emission involves a 578 cm^{-1} phonon. Because the two BEs experience very different carrier localizations, it is not surprising that they couple effectively to different phonons. While an E_u lattice mode, calculated by Fan[18] at 598 cm^{-1} and observed in absorption[31] at 580 cm^{-1} could be associated with the DBE indirect transition, it is also possible that the phonon coupling to the DBE is a local vibrational mode.

The optical transitions described in Fig. 2(b) are summarized in the level diagram of Fig. 3 as the wavy lines, with MC phonons indicated by the saw-toothed lines. The figure elucidates the relationship between the observed PL transition energies and the significant energy levels of the system. The DBE emission is represented as a ZPL.
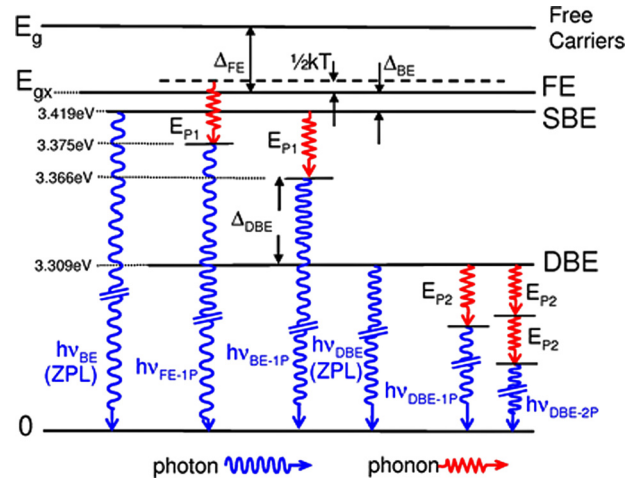

FIG. 3. Schematic level diagram indicating optical transitions as wavy lines and MC phonons as saw-toothed lines. The most prominent PL features in the exciton region are indicated, as well as low temperature PL peak positions and the characteristic exciton energy separations Δ_{FE}, Δ_{BE}, and Δ_{DBE}. The DBE line at 3.309 eV is assumed to be a ZPL.

C. Temperature dependence of the exciton spectra

The temperature dependence of the PL spectra in the exciton region is shown in Fig. 4 for sample B over the temperature range 8 K–294 K. The maximum intensity of each spectrum is normalized to the same height and shifted vertically, so that relative intensity variations can be compared directly. At the lowest temperatures, the spectra exhibit only the DBE and SBE emissions. As temperature is raised, the
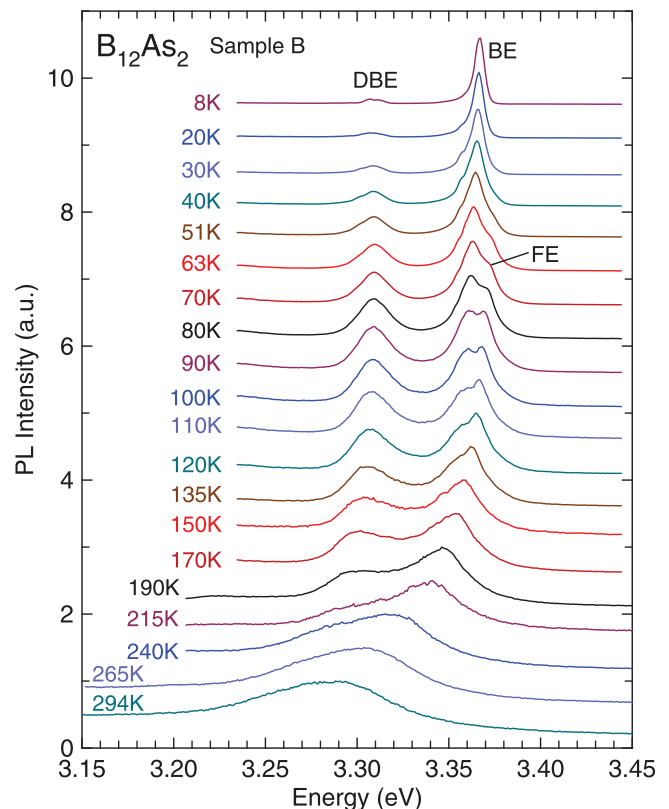

FIG. 4. Temperature dependence of the exciton PL spectra of sample B. All spectra are normalized to the same height and are shifted vertically.
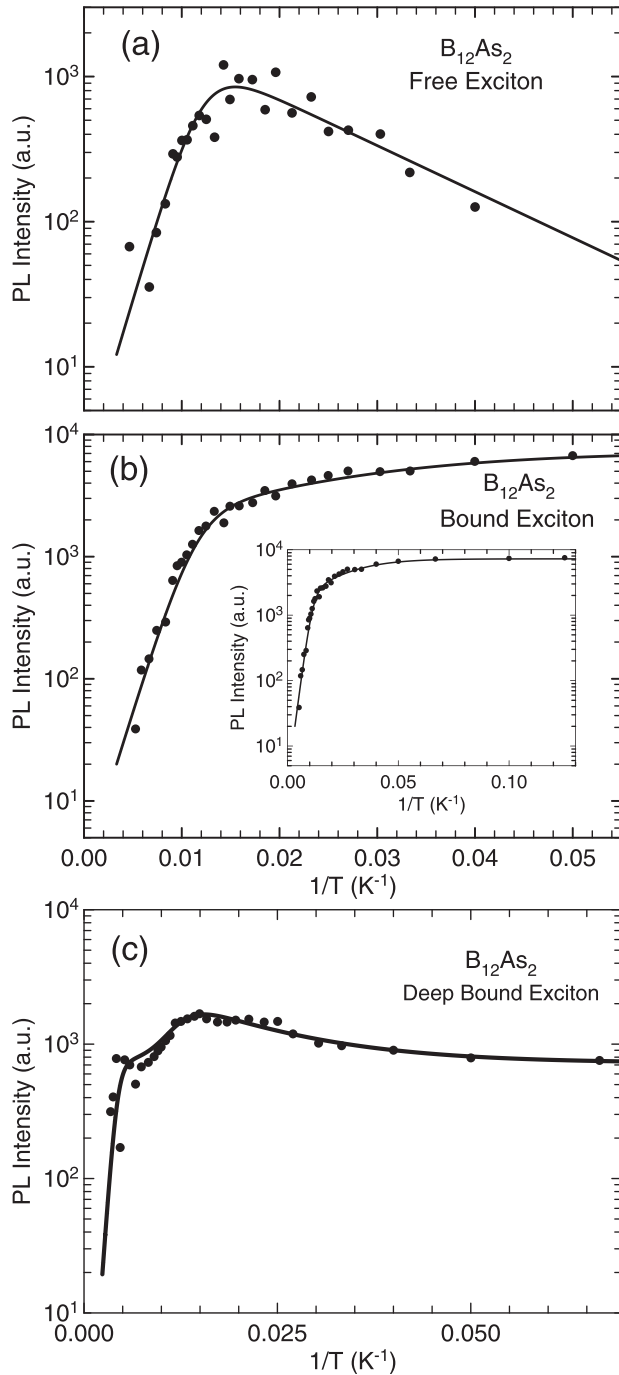
FIG. 5. Temperature dependence of the integrated PL intensities of the (a) FE, (b) SBE, and (c) DBE. The fits of the data to Eqs. (3), (4), and (5), respectively, appear as the solid lines. The inset in (b) extends to a broader temperature range.

absolute intensity of the SBE decreases slowly while that of the DBE begins to increase (see e.g. Fig. 5), so that their relative intensities begin to change. As the temperature increases beyond 25 K, a new band emerges from the high energy tail of the SBE line and increases in intensity relative to the SBE as temperature is further increased, becoming totally dominant above about 120 K. This is typical behavior for FE emission: At very low temperatures, the BE state is more stable. Therefore, unless the concentration of impurities that bind excitons is very low, FE emission at very low temperature is weak. As temperature is raised, FEs are thermally dissociated

from the BEs, thus increasing the FE concentration and the associated FE PL intensity and decreasing the corresponding SBE intensity. At higher temperatures, the dissociation of the FE into free carriers dominates and the FE intensity rapidly decreases with temperature. This dependence of the FE intensity on temperature consequently provides a measure of the FE binding energy, Δ_{FE}. Once Δ_{FE} is determined, the measured temperature dependence of the energy position of the FE PL peak (1-P replica), $h\nu_{FE-1P}$, provides the information necessary to determine the temperature dependence of the IBA bandgap (see, e.g., Fig. 3):

$$E_g(T) = [h\nu_{FE-1P}(T) - \tfrac{1}{2}kT] + \Delta_{FE} + E_{P1} = E_{gx}(T) + \Delta_{FE},$$
(1)

where E_{P1} is the energy of the MC phonon ($\approx$52.5 meV/ 423 cm^{-1}). $E_{gx}(T) = h\nu_{FE-1P}(T) - \tfrac{1}{2}kT + E_{P1}$ is the exciton gap energy (i.e., the position where the ZPL of the FE emission would appear). The factor $\tfrac{1}{2}kT$ comes from the FE PL lineshape, $I_{FE}(h\nu) \propto (h\nu - E_{gx})^{1/2}\exp[-(h\nu - E_{gx})/kT]$, which peaks $\tfrac{1}{2}kT$ higher in energy than the actual exciton gap.

The SBE is localized relative to the FE by the SBE localization energy Δ_{BE}. Since the peak of the FE PL band is at $\tfrac{1}{2}kT$ higher energy than the exciton gap, the separation of the FE and BE PL peaks is given by

$$[h\nu_{FE-1P}(T) - h\nu_{BE-1P}(T)] = \Delta_{BE} + \tfrac{1}{2}kT.$$
(2)

Consequently, we can obtain a measure of Δ_{BE} from the separation of these two peaks. In Sec. III E we find that $\Delta_{BE} = 6.3 \pm 1$ meV, independent of temperature.

To extract the temperature dependence of the DBE, SBE, and FE integrated intensities and peak positions from the overlapping spectral features in Fig. 4, the data were fitted using commercial peak fitting software.

D. Temperature-dependent intensities

The temperature dependent free and bound exciton intensities are determined by the steady-state balance of photoexcited carrier generation, radiative recombination, and the capture and thermal liberation of excitons from their bound states. Ping[35] has worked out a detailed model for the steady-state case, providing temperature-dependent expressions for the FE and SBE populations and PL intensities. These are of the form

$$I_{BE}(T) \propto \frac{1}{1 + Ae^{-\Delta_{BE}/kT} + Be^{-(\Delta_{BE} + \Delta_{FE})/kT}},$$
(3)

$$I_{FE}(T) \propto \frac{1 + Ce^{-\Delta_{BE}/kT}}{1 + Ae^{-\Delta_{BE}/kT} + Be^{-(\Delta_{BE} + \Delta_{FE})/kT}}.$$
(4)

The two ionization energies appearing in the exponents in Eqs. (3) and (4), correspond to the thermalization of the BE from the impurity, producing either a FE (Δ_{BE} term) or a free electron-hole pair ($\Delta_{BE} + \Delta_{FE}$ term). The A's, B's, and C's involve coefficients for carrier emission and radiative recombination from the various levels of the system. The coupling of all three levels (free carriers, FEs and BEs) through emission

and capture is responsible for the appearance of both exciton binding energies, Δ_{BE} and Δ_{FE}, in the expression for the intensity of each exciton emission. The measured temperature dependence of the spectrally integrated PL intensities for the FE and SBE are shown as the filled circles in Figs. 5(a) and 5(b), respectively. At low temperatures, the FE intensity initially increases with temperature as FEs are thermalized from BE's, while the BE intensity correspondingly decreases monotonically. At the highest temperatures, both excitons are thermalized directly into free electron-hole pairs. Both sets of data (FEs and BEs) can be fitted (solid lines) with Eqs. (3) and (4) using the same two exciton binding energies: $\Delta_{BE} = 6.3 \pm 1$ meV and $\Delta_{FE} = 45 \pm 5$ meV. The BE localization energy Δ_{BE} was not a fitting parameter but was determined directly from the separation of the FE and BE emission peaks, as noted in reference to Eq. (2) and described explicitly in Sec. III E. The fitting parameters (beyond an overall scaling factor) for the SBE were A = 4.5, B = 2600 and for the FE were A = 0.005, B = 1400, and C = 3000. The FE binding energy of 45 meV is somewhat lower than the 66 meV reported by Bakalova *et al.*,[36] determined from the effective masses evaluated[21] from first principles band structure calculations. This is discussed in detail in Sec. III F.

The temperature dependence of the DBE intensity is shown in Fig. 5(c). The PL intensity increases with increasing temperature until about 60 K and then decreases, qualitatively following the FE population, as in Fig. 5(a). This is suggestive of a DBE that forms by trapping FEs that have been thermalized from a SBE site. The DBE can also sequentially trap free carriers. We have extended Ping's approach slightly to add the DBE state to the steady-state model. Experimentally, this emission peak was shifted below the SBE peak by $\Delta_{DBE} \equiv h\nu_{SBE} - h\nu_{DBE} = 57$ meV. The steady-state DBE population is determined by radiative emission and by transitions between the DBE state and both free excitons and free carriers. Incorporating this into the model with the DBE line assumed to be a ZPL, the temperature dependence of the DBE population (and/or intensity) can be approximated, assuming a slow-varying free carrier concentration, in the form:

$$I_{DBE}(T) \propto \frac{1 + An_{FE}(T)}{1 + Be^{-(\Delta_{BE} + \Delta_{DBE} + E_{P1})/kT} + Ce^{-(\Delta_{BE} + \Delta_{DBE} + E_{P1} + \Delta_{FE})/kT}}.$$
(5)

Here, $n_{FE}(T)$ represents the FE population (e.g., Eq. (3)), while the two transition energies appearing in the exponents reflect the thermalization of the DBE state, leading (see, e.g., Fig. 3) to the liberation of either FEs ($\Delta_{BE} + \Delta_{DBE} + E_{P1}$) or free electron-hole pairs ($\Delta_{BE} + \Delta_{DBE} + E_{P1} + \Delta_{FE}$). The expression ($\Delta_{BE} + \Delta_{DBE} + E_{P1}$) corresponds to the DBE localization energy $E_{gx} - h\nu_{BE}$, ≈ 116 meV. The experimental data (filled circles) are shown in Fig. 5(c) fitted to Eq. (5) (solid line) using the same values of $\Delta_{BE} = 6.3$ meV and $\Delta_{FE} = 45$ meV as determined above and with $\Delta_{DBE} = 57$ meV and $E_{P1} = 52.5$ meV determined directly from the separation of spectral peak positions. The fitting parameters were A = 1.54×10^{-3}, B = 20, and C = 3000.

If the alternative view is taken that the 3.309 eV DBE PL is a 1-P replica, with ZPL at 3.381 eV (not observed), then the DBE localization energy would be reduced by $E_{P2} = 71.6$ meV to ≈ 44 meV—which is still a large BE binding energy. As the temperature dependence in Fig. 5(c) is dominated by $n_{FE}(T)$, a similar fit of the data may be obtained with this reduced DBE localization. Consequently, the lack of an observed ZPL results in some ambiguity regarding the DBE localization energy, and both values are entered in the summary of IBA material parameters appearing in Table II.

With the FE binding energy of 45 ± 5 meV measured from the temperature dependent FE PL intensity, the temperature dependence of the indirect band gap can now be considered.

E. Temperature dependence of the energy gap

The temperature dependence of the energy positions of the FE, SBE, and DBE determined from the peak-fitting analysis of the temperature dependent spectra is shown plotted in Fig. 6(a) as the filled triangles, squares, and circles, respectively. It is apparent that the peak position of the exciton, unlike that of the SBE and FE, is unaffected by the temperature dependence of the band gap, up to temperatures greater than 100 K. This is behavior consistent with a exciton that is strongly coupled to a deep binding center: Patrick and Choyke[37] investigated DBEs due to Ti impurities in several SiC polytypes and interpreted the independence of the DBE recombination energy from the position of the band edge as characteristic of excitons that involve the localized d-electrons of the transition metal. Similarly, Kimoto *et al.*[34] reported Ti-related DBE emission in Ti:6H-SiC that exhibited no variation in spectral position over a wide temperature range (14-77 K). Similar behavior would be expected from excitons bound to other transition metals. Thus, the temperature independence of the DBE energy suggests the possibility of a Ni-related DBE.

At the bottom of the figure the measured energy differences between the FE and SBE peak energies are plotted as

TABLE II. Experimental IBA material parameters.

| Parameter	Description	Value
$E_g(0)$	Low temperature gap	3.470 ± 0.005 eV
$E_g(294\,K)$	Room temperature gap	3.373 ± 0.01 eV
$E_g(T)$	Temp. dep.—Varshni	$3.470 \pm 0.005 - 4 \times 10^{-4}T^2/(640 - T)$ eV
	Temp. dep.—Pässler	$3.470 \pm 0.005 - 0.90\{[1 + (T/450)]^{2.7} - 1\}^{(1/2.7)}$ eV
Δ_{BE}	BE localization energy	6.3 ± 1 meV
Δ_{FE}	FE localization energy	45 ± 5 meV
$E_{gx} - h\nu_{DBE}$	DBE localization energy	116 meV DBE = ZPL
		44 meV DBE = 1 − P replica
E_D	Donor binding energy	25 ± 10 meV
E_A	Acceptor binding energy	175 ± 25 meV
		255 ± 25 meV
		291 ± 25 meV
E_{P1}	MC phonon—SBE	52.5 meV/423 cm^{-1}
E_{P2}	MC phonon—DBE	71.6 meV/578 cm^{-1}
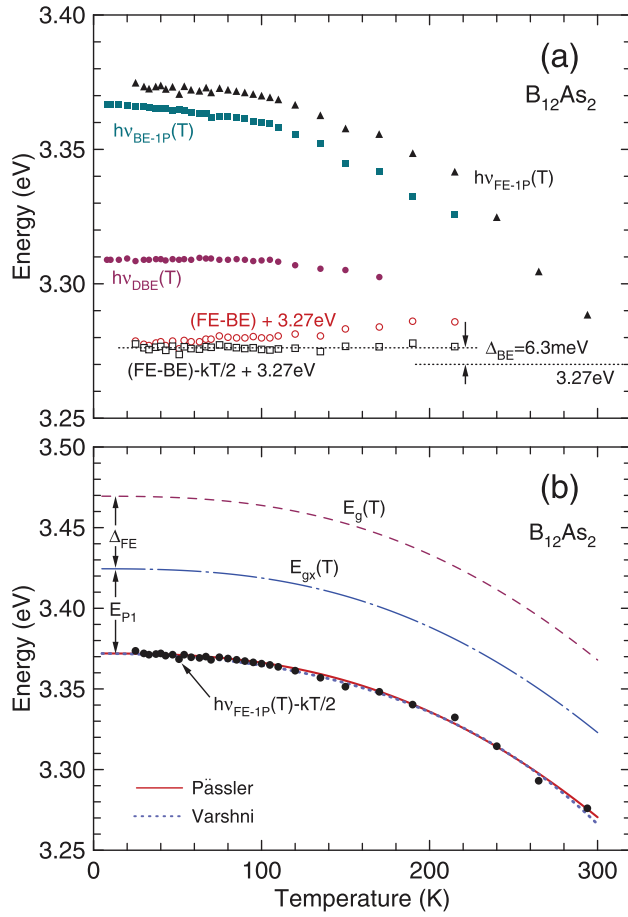
FIG. 6. (a) Temperature dependence of the positions of the FE-1P [$h\nu_{FE\text{-}1P}$ (T), filled triangles], SBE-1P [$h\nu_{BE\text{-}1P}$(T), filled squares], and DBE (filled circles). The energy separation between the FE and SBE lines is shown as the open circles and is shifted up by 3.27 eV to appear on the same scale. Subtracting ½kT from this (Eq. (2)) gives the SBE localization energy Δ_{BE} (open squares) of 6.3 meV. (b) The FE-1P exciton gap, $h\nu_{FE\text{-}1P}$(T) $-$ ½kT, is plotted as the filled circles, and is fitted with both Varshni (dotted line) and Pässler (solid line) expressions. This fit is also shown shifted up by 52.5 meV (MC phonon energy) to represent the exciton gap E_{gx}(T) (dash-dot line) and by an additional 45 meV (FE binding energy) to represent the indirect band gap (dashed line at the top).

open circles. These are shifted up by 3.27 eV in the figure, so as to appear on the same scale. The data show a separation between the two peaks that increases slowly with temperature, as expected from the ½kT term in Eq. (2). Δ_{BE} is determined by subtracting ½kT from this data, which is shown as the open squares and results in a temperature independent BE localization energy $\Delta_{BE} = 6.3 \pm 1$ meV.

Following the FE PL up to room temperature provided data that could be fitted over almost the entire temperature range (25-294 K). The phonon-assisted FE gap, $h\nu_{FE\text{-}1P}$(T) $-$ ½kT, is plotted as the filled circles in Fig. 6(b) and was fitted with the ad hoc Varshni equation,[38] $E_{FE\text{-}1P}(T) = E_{FE\text{-}1P}(0) - aT^2/(T+b)$ as the dotted line through the FE data points, with $E_{FE\text{-}1P}(0) = 3.372$ eV, $a = -4 \times 10^{-4}$ eV/K and $b = -640$ K. IBA exhibits negative Varshni coefficients, similar to some other wide bandgap semiconductors, such as 6H-SiC and diamond.[39] While the empirical Varshni equation has been the expression most commonly used to fit the temperature dependent band gap, more accurate models have been proposed that have the advantage of depending on real

physical parameters. A model developed by Pässler[40] has recently been employed successfully by Grivickas *et al.*[41] to fit the temperature dependent absorption edge of 4H-SiC. While the formal Pässler expression is somewhat complicated, in the low-dispersion limit a very good approximation[42] takes the form $E(T) = E(0) - (\alpha\Theta_p/2)\{[1 + (2\,T/\Theta_p)^p]^{1/p} - 1\}$. Here, α is the slope of E vs. T at the high temperature limit, Θ_p is the average phonon temperature, and p is related to the degree of phonon dispersion Δ by $p = (1 + 1/\Delta^2)^{1/2}$. The fit of the FE data in Fig. 6(b) using this model, which was essentially identical to that using the full expression, is given as the solid line through the FE data points, with $E_{FE\text{-}1P}(0) = 3.372$ eV, $\alpha = 2 \times 10^{-3}$ eV/K, $\Theta_p = 900$ K, and $\Delta = 0.40$ (or p = 2.7). At low temperature and room temperature, the fit to the data gave $E_{FE\text{-}1P}(0) = 3.372$ eV and $E_{FE\text{-}1P}(294\,K) = 3.275$ eV.

Except for $E_g(0)$, the Pässler parameters for the indirect band gap also apply to those determined for the FE-1P data. By shifting this fit of the FE data up by one MC phonon energy (52.5 meV) (see, e.g., Eq. (1)), the temperature dependence of the exciton band gap E_{gx}(T) is obtained and is given by the dotted-dashed line in the figure. Adding to this, the FE binding energy of 45 ± 5 meV gives the temperature dependence of the indirect band gap, E_g(T), indicated in Table II and shown as the dashed curve at the top of the figure. From this fit, the indirect energy gap of IBA at T = 0 and at room temperature is obtained:

$$E_g(0) = 3.470 \pm 0.005\,\text{eV},$$
$$E_g(294\ \text{K}) = 3.373 \pm 0.01\ \text{eV}. \tag{6}$$

Since the fitted FE binding energy involves a 5 meV uncertainty and contributes additively to the low temperature band gap, this uncertainty also applies to $E_g(0)$. However, this corresponds to a rigid energy shift of E_g(T) and does not significantly affect the temperature dependence. Obtaining the room temperature band gap required a fit of the data to the Pässler expression and a total uncertainty in $E_g(294\,K)$ of <10 meV is estimated at room temperature.

The $\approx 3.37 \pm 0.01$ eV room-temperature band gap appears in between the two previous reports of 3.20 eV and 3.47 eV. The former was determined primarily from a band structure calculation, as the ellipsometry measurements near the indirect band edge were dominated by impurity absorption.[21] This value of 3.20 eV for the indirect band gap is inconsistent with the present PL data, however, as the entire 294 K near-bandedge PL spectrum in Fig. 4 lies well above this energy. The 100 meV discrepancy between the PL and the optical absorption results is rather large. To investigate this further the published data of Slack *et al.*[24] have been digitized. This data were originally presented in the form of absorption coefficient vs. photon energy: α vs. $h\nu$. However, indirect absorption is usually plotted as $\alpha^{1/2}$ vs. $h\nu$ to reflect a linear dependence. The original data of Ref. 24 has been re-plotted in this format as the heavy solid line in Fig. 7 and the positions of the three proposed indirect gap energies are indicated. The dashed line is our linear extrapolation of the absorption data that leads to an intercept with the energy axis at 3.47 eV, similar to what was obtained by Slack *et al.* There is, however, a low energy tail,
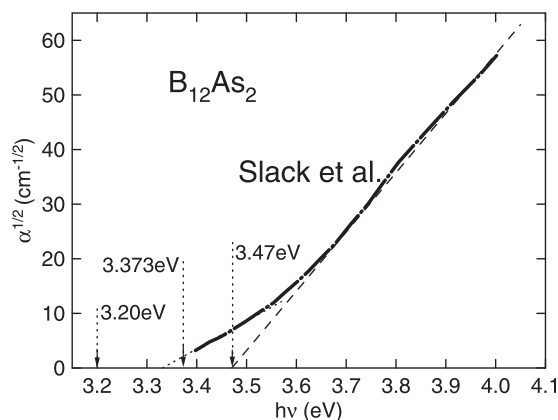
FIG. 7. Digitized optical absorption data of Ref. 24 (solid line), plotted as $\alpha^{1/2}$ vs. hν. The dashed line represents a linear extrapolation with a threshold at 3.47 eV, and the three indirect band gaps under consideration are indicated by the arrows. An extrapolation of the tail region is given by the dotted line.

which might be interpreted as either impurity absorption, indirect absorption, or a combination of the two. A linear extrapolation of the tail region (dotted line), assuming indirect absorption, leads to an intercept at about 3.33 eV, well below the 3.37 eV band gap determined here. Consequently, we believe this absorption tail to be primarily due to impurity absorption, similar to that encountered by Bakalova *et al.*,[21] which masks the indirect absorption at hν ≥ 3.37 eV. The main absorption threshold fitted by Slack *et al.* occurs at 3.47 eV, which is in excellent agreement with the lowest *direct* absorption at 3.46 eV reported by Bakalova *et al.*[21] While this absorption does appear to exhibit a linear $\alpha^{1/2}$ vs. hν dependence above about 3.6 eV, the available evidence suggests that the original determination of the indirect absorption edge was probably fitted to a direct transition. In their original paper, Slack *et al.* stated that impurity absorption was assumed negligible. However, the existence of a tail region (Fig. 7) should have clearly indicated either impurity absorption or a much lower indirect band edge.

Note that if the main SBE and associated FE PL bands were interpreted as ZPLs instead of 1P-replicas, so that a MC phonon energy was *not* added to the measured FE line positions in determining $E_g(T)$, then a room temperature band gap of ≈3.32 eV would have been obtained. This would be in excellent agreement with the extrapolated tail region of the Slack *et al.* absorption data, and the absorption tail would consequently be assigned as the indirect absorption edge. This would lead to a ≈3.32 eV room temperature indirect band gap and would provide a consistent explanation of both the old absorption data and the new PL data. While this would make for a very satisfying picture, it is difficult to ignore the correspondence between the main SBE line at 3.366 eV and the weak 3.419 eV feature in Fig. 2(a), which requires that the dominant BE feature be assigned as a 1-P replica, placing the room temperature band edge at ≈3.37 eV.

F. Donor-acceptor pair spectra

The DAP region, ≈3.0–3.3 eV, is dominated by three broad peaks centered near 3.094, 3.13, and 3.21 eV. The DAP
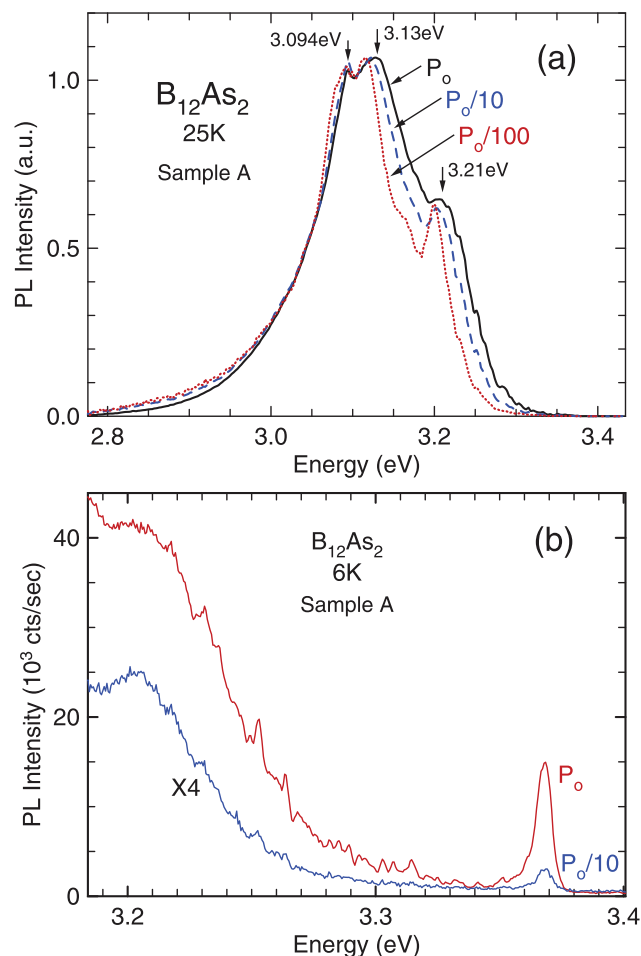

FIG. 8. (a) Dependence of the DAP spectrum of sample A on excitation power. The peak intensities are all normalized to the same height. (b) The high energy edge of the DAP spectrum shown at low and high laser power. The sharp and reproducible features in the high power spectrum reflect recombination from close DAPs at discrete donor-acceptor separations.

nature of the emission becomes apparent from the dependence of the spectrum on excitation power. In Fig. 8(a), we compare three spectra (with all peak intensities normalized to the same amplitude) obtained using relative laser powers of 1.0, 0.1, and 0.01. With decreasing power, the high energy edge of the two higher energy lines shifts to lower energy—one of the hallmarks of DAP recombination.[43] The apparent peak positions are affected by both the varying high energy edge and the varying sloped backgrounds that are due to the lower energy DAPs. Consequently, the shifts in position of some of the peaks do not follow the shift in the high energy edge in a linear fashion. As we cannot see the high energy edge for the lowest 3.094 eV band, we can only assume by its proximity to the other lines that it is also of DAP origin. As the three lines were observed to exhibit different dependences upon temperature (see Fig. 9), they do not appear to be different phonon replicas of a single pair band, but instead represent independent impurity pairs. As there has not been a previous report of a donor in IBA, it is most likely that the three lines represent three different acceptors. Also, since IBA is an indirect gap material, the DAP emission could also involve a momentum-conserving phonon. However, no associated ZPL was identified.
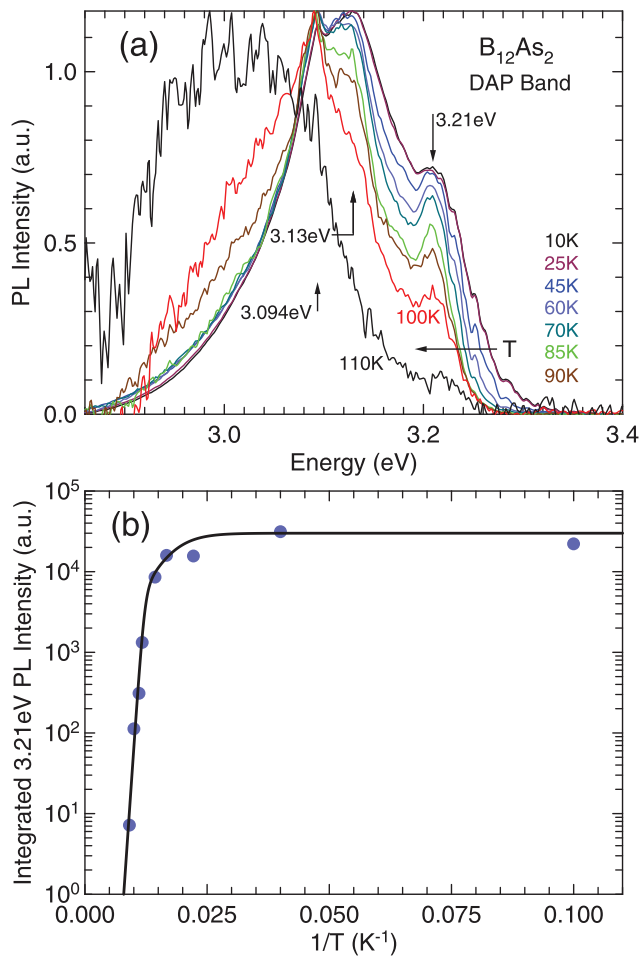
FIG. 9. (a) Temperature dependence of the DAP spectrum between 10 K and 110 K. Peak intensities are all normalized to the same height, corresponding to the intensity of the deepest DAP feature at 3.094 eV, except for the 110 K data. The intensities of the higher energy lines, corresponding to shallower impurities, are seen to decrease with increasing temperature faster than the deeper bands. (b) Temperature dependence of the integrated intensity of the 3.21 eV band. The solid line is a fit of the data to Eq. (8).

The high-energy edge of the DAP region of sample A is shown in Fig. 8(b) for two power levels differing by an order of magnitude. A series of sharp, reproducible emission bands extending from the broad distant-pair band ($\approx$3.21 eV) to higher energy are apparent at high excitation and are considerably reduced at lower power. These represent recombination between close donor-acceptor pairs at discrete DAP separations,[43] similar to those observed in BP,[44] SiC,[45] and GaP.[46] The observation of a close-pair spectrum further confirms the DAP origin of the 3.0-3.3 eV region. While we cannot yet identify the donor and acceptor species responsible for the observed PL emission, the existence of a DAP band provides evidence of a donor in IBA, which is of considerable interest, as n-type material has not yet been reported.

In β-rhombohedral boron, Ni as well as several other transition metals were shown to be effective as n-type dopants[47,48] that incorporate on an interstitial site of the boron icosahedron.[48] Ni also acts as an n-type dopant in boron carbide[49] and in boron-carbon alloys.[50] Given the high concentration of Ni in these IBA samples (Table I) and the fact that the structure of IBA shares the boron icosahedron with these

compounds, it is likely that the donor in question is an interstitial Ni impurity.

The possibility of a Ni donor in IBA is discussed in more detail below. However, since a Ni-related DBE was already suggested in an earlier section, some further comment seems appropriate. For both the shallow donor and the DBE, it should be made clear that no evidence is presented that definitely identifies Ni with either of these two centers. There is sufficient circumstantial evidence presented, however, to justify serious consideration of the role of Ni in both of these cases. The shallow donor and the DBE would correspond to Ni incorporation at different sites, which would certainly not be surprising, given the large Ni concentration in these samples.

Since electrical measurements have not been carried out in the present samples, and with the high concentration of Ni impurities, we cannot be sure if the samples are p-type, as they usually are, or n-type. We also have no direct information about the compensation level in these samples. However, the observation of relatively sharp exciton structure at low temperature is not consistent with a high concentration of free carriers. This suggests that the material is highly compensated and/or that only a small fraction of the Ni impurities incorporate as interstitial donors in the boron icosahedra. Also, since the PL measurements were restricted to the high quality region of each sample, the Ni concentrations in these regions may be much lower than what was indicated in Table I. Evidence of significant compensation is observed, however, in the SBE lineshape in Fig. 2(a), which exhibits a clear asymmetric tail at lower energies. This BE lineshape has been associated both theoretically[51] and experimentally[52] with the Stark effect due to ionized impurities. The lineshape in Fig. 2(a) could be fitted to the model in Ref. 51, which provided a rough estimate of the ionized impurity concentration, $\approx 2 \times 10^{18}$ cm^{-3}. However, in order to confirm the role of Ni in the transport properties of IBA, a combination of electrical and optical measurements on samples with carefully controlled Ni concentrations will be required.

To obtain an estimate of the donor and acceptor binding energies, the DAP spectrum was studied as a function of temperature. In general, the measured photon energy hν_{DAP} emitted by an indirect band gap material through a DAP transition between neutral donors and acceptors separated by a distance r is given by

$$h\nu_{DAP}(r) = E_g - (E_D + E_A) + e^2/\varepsilon r - E_P, \qquad (7)$$

where E_g, E_D, and E_A are the band gap and donor and acceptor binding energies, respectively, $e^2/\varepsilon r$ is the Coulomb interaction between the two ionized impurities of the final state, with e the electronic charge and ε the static dielectric constant. E_P is the energy of the MC phonon. Fig. 9(a) shows DAP spectra taken between 10 K and 110 K, with the intensities (monotonically decreasing with temperature) all normalized to the same peak height. It is apparent, as noted earlier, that the 3.21 eV, 3.13 eV, and 3.094 eV peaks exhibit different dependences on temperature, with the highest energy emissions decreasing more rapidly with temperature than the deeper bands. This is exactly what is expected from

the temperature dependence of DAP PL involving more than one acceptor (or donor): The highest energy emission corresponds to the shallowest acceptor (donor), which thermalizes first, before the deeper impurities.

At higher temperatures (≥ 90 K), a broad band centered near 3.0 eV and with intensity decreasing much more slowly with temperature than the DAP band emerged from the low-energy tail of the DAP and had a significant effect on the low energy portion of the DAP spectrum at these temperatures. This band totally dominates the 110 K spectrum in Fig. 9(a). While its origin is unidentified at present, the large line width suggests recombination at a defect center.

To extract the temperature dependence of the DAP intensities, it is necessary to separate the contributions from the three individual peaks (as well as the 3.0 eV band). Because the two lowest energy peaks in the DAP spectra are relatively close together, it was not possible to reliably deconvolute these bands. However, the 3.21 eV peak is well separated from the others and could be successfully separated from the background of the other lines, which allowed its integrated intensity to be determined as a function of temperature. This dependence is shown as the filled circles in Fig. 9(b). The data are fitted with two ionization paths, corresponding to the sequential thermalization of the donor and the acceptor:

$$I_{DAP}(T) \propto \frac{1}{1 + Ae^{-E_D/kT} + Be^{-E_A/kT}}. \tag{8}$$

The best fit to the data in Fig. 9(b), assuming that $E_A > E_D$, was obtained with $E_A = 175 \pm 25$ meV, $E_D = 25 \pm 10$ meV. Using the measured separations between the 3.21 eV band and the other two deeper DAP lines, we estimate acceptor binding energies of 255 meV and 291 meV for the two deeper acceptors.

Recent Hall effect measurements[15] on heteroepitaxial layers of IBA on semi-insulating 6H-SiC substrates found the as-grown layers to be p-type. Three shallow acceptor activation energies were reported at 150, 260, and 330 meV. This agrees well with the acceptor binding energies of 175, 255, and 291 meV obtained from the DAP PL spectra and further supports a DAP band derived from three distinct acceptors and a single donor. That the donor is the shallower of the two impurities is also consistent with the electron effective mass calculated by Bakalova *et al.*[21] ($m_e^* = 0.29$), which was considerably less than the corresponding hole masses. It is also noteworthy that the fitted donor binding energy of 25 meV is substantially lower than that expected from an effective mass donor: $E_D = m_e^* R_H/\varepsilon^2 \cong 64$ meV, where m_e^* and R_H represent the electron effective mass[21] and the hydrogen Rydberg, 13.6 eV, respectively, and $\varepsilon = 7.84$ (Ref. 21). Such a small binding energy is consistent with an interstitial donor impurity, such as the Ni impurity suggested above. Interstitial shallow impurities with binding energies considerably smaller than that predicted by effective mass theory have been reported in the literature. Some examples are Li and Na interstitials in ZnSe,[53] Cl interstitials in CuGaS$_2$,[54] and Zn interstitials in ZnO.[55] In the case of the latter, the deviation from effective mass theory was associated with the non-spherical charge distribution around the impurity site.

Thus, the temperature dependence of the intensity of the shallowest DAP band at 3.21 eV corresponds to shallow impurities with $E_D + E_A \approx 200 \pm 30$ meV. We can make an independent estimate of $E_D + E_A$ by employing Eq. (7), using $E_g = 3.47$ eV, $h\nu_{DAP} = 3.21$ eV, and $E_P = 52.5$ meV. Dean[43] has given an estimate of the DAP separation corresponding to the peak of the distant DAP band: $r_{pk} \cong (1/2\pi N)^{-1/3}$, where N is the concentration of the dominant impurity. For N in the range 10^{16}–10^{18} cm^{-3}, the corresponding Coulomb energy is in the range (5-21) meV. Equation (7) then gives: $(E_D + E_A) = (213\text{-}229)$ meV for $E_P = 52.5$ meV and $(E_D + E_A) = (265\text{-}281)$ meV for $E_P = 0$ (i.e., if no MC phonon is involved). The experimental result of $(E_D + E_A) \cong 200 \pm 30$ meV $= (170\text{-}230)$ meV is consistent with a DAP emission that is *phonon-assisted*, employing a 52.5 meV phonon. While no ZPLs were identified for the three DAP bands, the ZPL positions would be projected to be at 3.146, 3.182, and 3.262 eV.

Within the effective mass approximation, the acceptor binding energy is related to the hole effective mass through $E_A = m_h^* R_H/\varepsilon^2$. With the measured acceptor binding energy for the 3.21 eV band in the range $E_A = (150\text{-}200)$ meV, we find the corresponding m_h^* in the range (0.68-0.90). This is in stark contrast to the huge heavy-hole effective mass of $m_{hh}^* = 359$ calculated for the Γ-point in Ref. 21. Combining $m_h^* = 0.68\text{-}0.90$ with $m_e^* = 0.29$, we can obtain an estimate of the reduced mass m_r^* necessary to calculate the FE binding energy, $1/m_r^* = 1/m_e^* + 1/m_h^*$, with the result that $m_r^* = (0.203\text{-}0.219)$. The corresponding FE binding energy, $\Delta_{FE} = m_r^* R_H/\varepsilon^2$, is then in the range (45-48.5) meV, which is in much better agreement with the measured FE binding energy than the 66 meV calculated in Ref. 36 assuming an infinite hole mass.

The experimental data indicate that the DAP spectrum involves relatively shallow acceptors and that the FE binding energy estimated above from the shallow acceptor binding energy is in good agreement with experiment. On the other hand, the very large heavy-hole effective mass determined from the band structure calculations simply reflects a very flat valence band. This was also a feature of several earlier band structure calculations for IBA (Refs. 20–22) and is presumably accurate. However, such a large hole mass cannot support a shallow acceptor. This suggests that the observed shallow acceptors might be associated with the light-hole band. Bakalova *et al.*[21] calculated a light-hole mass of $m_{lh}^* = 0.46$. This corresponds to an effective mass acceptor binding energy of 102 meV. Given that m_{lh}^* has not been measured directly, and that the fitted binding energy of the shallowest acceptor, 150-200 meV, undoubtedly contains some central cell contribution, this could be considered as reasonable agreement. Using the calculated light-hole mass gives a reduced mass for the FE of $m_r^* = 0.178$ and a FE binding energy of $\Delta_{FE} = 39.4$ meV, which is also in reasonable agreement with experiment. Consequently, we conclude that, due to the very large heavy-hole mass, the observed shallow acceptors and the FE are probably associated with the light-hole band.

IV. SUMMARY

PL spectroscopy was carried out on solution-grown IBA crystals in the range 1.75-3.5 eV and over the temperature range 8 K-294 K in order to measure the indirect band gap and to investigate the shallow impurities in the material. The spectra were dominated by recombination due to deep defects, shallow donor-acceptor pairs, and excitons bound to both deep and shallow centers. Analysis of the temperature dependence of the PL intensities and line positions provided several material parameters, including the temperature dependence of the energy gap and the binding energies of the excitons and shallow donors and acceptors. These are summarized in Table II.

The dominant SBE emission was shown to involve a phonon-assisted transition, while the strongest DBE line appeared to be a ZPL, as no ZPL at higher energy could be observed. FE recombination was observed for temperatures ≥25 K and became the dominant feature in the spectrum by 120 K. The temperature dependence of the PL intensity of the FE provided the FE binding energy (45 meV), which was a necessary parameter to determine the indirect band gap.

The shift of the energy position of the phonon-assisted FE line with temperature reflects the temperature dependence of the indirect band gap and was fitted with both Varshni and Pässler expressions. The resulting indirect band gap at low- and room-temperatures was determined as 3.470 eV and 3.373 eV, respectively. This room temperature band gap is in contrast to two previously published values for the indirect gap: 3.20 eV (band structure calculation) and 3.47 eV (optical absorption). The former was found inconsistent with the observed room temperature PL spectra. A re-examination of the original optical absorption spectra, coupled with recent ellipsometry measurements, suggests that the optical absorption data appear to have been fitted to the lowest *direct* transition rather than the indirect edge, which may have been masked by impurity absorption.

A strong deep bound exciton emission was observed at 3.309 eV. The temperature dependence of the DBE spectrum reflected a peak position that was independent of temperature up to >100 K. This behavior is reminiscent of earlier reports of DBEs bound to transition metals and suggests the possible involvement of a Ni-related site in the origin of the DBE.

DAP spectra were identified through their dependence on excitation power, temperature and by the appearance of discrete DAP emission from close pairs. Three distant DAP bands were observed and were associated with three different acceptors. The observation of DAP emission in IBA indicates the presence of a donor. This is a significant finding, as n-type material has not yet been reported. While the identity of the donor impurity remains unknown, it is suggested that the donor may result from a fraction of the large Ni concentration, incorporated on interstitial sites of the boron icosahedron. Ni doping has produced n-type material (via a Ni interstitial) in other compounds incorporating boron icosahedra, and the small observed donor binding energy observed in IBA is consistent with an interstitial donor. The temperature dependence of the intensity of the shallowest DAP band provided estimates of the donor and acceptor binding energies (see Table II). However, the very large heavy-hole effective mass reported from recent band structure calculations cannot support such shallow acceptors. The results are, therefore, interpreted as due to acceptors associated with the light-hole band.

[1]D. Emin, Phys. Today **40**, 55 (1987).
[2]D. Emin, J. Solid State Chem. **179**, 2791 (2006).
[3]M. Carrard, D. Emin, and L. Zuppiroli, Phys. Rev. B **51**, 11270 (1995).
[4]G. A. Slack, D. W. Oliver, and F. H. Horn, Phys. Rev. B **4**, 1714 (1971).
[5]Z. Xu, J. H. Edgar, and S. Speakman, J. Cryst. Growth **293**, 162 (2006).
[6]Y. Zhang, H. Chen, M. Dudley, Y. Zhang, J. H. Edgar, Y. Gong, S. Bakalova, M. Kuball, L. Zhang, D. Su, and Y. Zhu, MRS Proc. **1307**, mrsf10-1307-cc02-03 (2011).
[7]H.Chen, G. Wang, M. Dudley, L. Zhang, Y. Zhu, Z. Xu, J. H. Edgar, and M. Kuball, J. Appl. Phys. **103**, 123508 (2008).
[8]H. Chen, G. Wang, M. Dudley, Z. Xu, J. H. Edgar, T. Batten, M. Kuball, L. Zhang, and Y. Zhu, Appl. Phys. Lett. **92**, 231917 (2008).
[9]C. E. Whiteley, Y. Zhang, Y. Gong, S. Bakalova, A. Mayo, J. H. Edgar, and M. Kuball, J. Cryst. Growth **318**, 553 (2011).
[10]J. R. Michael, T. L. Aselage, D. Emin, and P. G. Kotula, J. Mater. Res. **20**, 3004 (2005).
[11]T. L. Aselage, D. R. Tallant, and D. Emin, Phys. Rev. B **56**, 3122 (1997).
[12]J. W. Pomeroy, M. Kuball, H. Hubel, N. W. A. van Uden, D. J. Dunstan, R. Nagarajan, and J. H. Edgar, J. Appl. Phys. **96**, 910 (2004).
[13]Y. Gong, M. Tapajna, S. Bakalova, Y. Zhang, J. H. Edgar, Y. Zhang, M. Dudley, M. Hopkins, and M. Kuball, Appl. Phys. Lett. **96**, 223506 (2010).
[14]Z. Xu, J. H. Edgar, D. C. Look, S. Baumann, R. J. Bleiler, S. H. Wang, and S. E. Mohney, J. Appl. Phys. **101**, 053710 (2007).
[15]Y. Zhang, Ph.D. thesis, Kansas State University, 2011.
[16]Y. Gong, Y. Zhang, M. Dudley, Y. Zhang, J. H. Edgar, P. J. Heard, and M. Kuball, J. Appl. Phys. **108**, 084906 (2010).
[17]C. L. Beckel, N. Lu, B. Abbott, and M. Yousaf, Inorg. Chim. Acta **289**, 198 (1999).
[18]Z. Fan, B. Wang, X. Xu, X. Cao, and Y. Wang, Phys. Status Solidi B **248** 1242 (2011).
[19]D. R. Armstrong, J. Bolland, and P. G. Perkins, Theor. Chim. Acta **64**, 501 (1984).
[20]I. Morrison, D. M. Bylander, and L. Kleinman, Phys. Rev. B **45**, 1533 (1992).
[21]S. Bakalova, Y. Gong, C. Cobet, N. Esser, Y. Zhang, J. H. Edgar, Y. Zhang, M. Dudley, and M. Kuball, Phys. Rev. B **81**, 075114 (2010).
[22]D. Li and W. Y. Ching, Phys. Rev. B **52**, 17073 (1995).
[23]D. R. Tallant, T. L. Aselage, and D. Emin, AIP Conf. Proc. **231**, 301 (1991).
[24]G. A. Slack, T. F. McNelly, and E. A. Taft, J. Phys. Chem. Solids **44**, 1009 (1983).
[25]R. Armitage, W. Hong, Q. Yang, H. Feick, J. Gebauer, E. R. Weber, S. Hautakangas, and K. Saarinen, Appl. Phys. Lett. **82**, 3457 (2003).
[26]A. Kakanakova-Georgieva, U. Forsberg, and E. Janzén, Phys. Status Solidi A **208**, 2182 (2011).
[27]S. G. Sridhara, L. L. Clemen, R. P. Devaty, W. J. Choyke, D. J. Larkin, H. S. Kong, T. Troffer, and G. Pensl, J. Appl. Phys **83**, 7909 (1998).
[28]D. Bimberg, M. Sondergeld, and E. Grobe, Phys. Rev. B **4**, 3451 (1971).
[29]R. Ruhle, W. Schmid, R. Meck, N. Stath, J. U. Fischbach, I. Strottner, K. W. Benz, and M. Pilkuhn, Rev. B **18**, 7022 (1978).
[30]D. R. Hamilton, W. J. Choyke, and L. Patrick, Phys. Rev. **131**, 127 (1963).
[31]H. Stein and A. Stintz, work reported by Beckel *et al.* in Ref. 17.
[32]D. J. Robbins and P. J. Dean, Adv. Phys. **27**, 499 (1978).
[33]S. G. Bishop, P. J. Dean, P. Porteous, and D. J. Robbins, J. Phys. C **13**, 1331 (1980).
[34]T. Kimoto, H. Nishino, T. Ueda, A. Yamashita, W. S. Yoo, and H. Matsunami, Jpn. J. Appl. Phys. **2B**, L289 (1991).
[35]Er -Xuan Ping, Appl. Phys. Lett. **62**, 493 (1993).

[36]S. Bakalova, Y. Gong, C. Cobet, N. Esser, Y. Zhang, J. H. Edgar, Y. Zhang, M. Dudley, and M. Kuball, J. Phys. Condens. Matter **22**, 395801 (2010).

[37]L. Patrick and W. J. Choyke, Phys. Rev. B **10**, 5091 (1974).

[38]Y. P. Varshni, Physica **34**, 149 (1967).

[39]J. I. Pankove, *Optical Processes in Semiconductors* (Dover, New York, 1971), p. 27.

[40]R. Pässler, Phys. Rev. B **66**, 085201 (2002).

[41]P. Grivickas, V. Grivickas, J. Linnros, and A. Galeckas, J. Appl. Phys. **101**, 123521 (2007).

[42]R. Pässler, Phys. Status Solidi B **200**, 155 (1997).

[43]P. J. Dean, Prog. Solid State Chem. **8**, 1 (1973).

[44]F. M. Ryan and R. C. Miller, Phys. Rev. B **148**, 858 (1966).

[45]J. A. Freitas, Jr., S. G. Bishop, P. E. R. Nordquist, Jr., and M. L. Gipe, Appl. Phys. Lett. **52**, 1695 (1988).

[46]P. J. Dean, C. J. Frosch, and C. H. Henry, J. Appl. Phys. **39**, 5631 (1968).

[47]H. Werheit, R. Schmechel, V. Kueffel, and T. Lundstrom, J. Alloys Compd. **262–263**, 372 (1997).

[48]H. Werheit, K. De Groot, W. Malkemper, and T. Lundstrom, J. Less-common Met. **82**, 163 (1981).

[49]S.-D. Hwang, N. B. Remmes, and P. A. Dowben, J. Vac. Sci Technol. B **14**, 2957 (1996).

[50]D. N. McIlroy, S.-D. Hwang, K. Yang, N. Remmes, P. A. Dowben, A. A. Ahmad, J. J. Ianno, J. Z. Li, J. Y. Lin, and H. X. Jiang, Appl. Phys. A **67**, 335 (1998).

[51]E. Hanamura, J. Phys. Soc. Jpn. **28**, 120 (1970).

[52]H. Kukimoto, S. Shionoy, S. Toyotomi, and K. Morigaki, J. Phys. Soc. Jpn. **28**, 110 (1970).

[53]G. F. Neumark, Phys. Rev. B **37**, 4778 (1988).

[54]M. Morohashi, Y. Ando, N. Tsuboi, T. Terasako, S. Iida, and S. Okamoto, Jpn. J. Appl. Phys. **32** (Suppl. 32-3), 621 (1993).

[55]Y. Sun and H. Wang, Physica B **325**, 157 (2003).